# Spectroscopic, topological, and electronic characterization of ultrathin *a*-CdTe:O tunnel barriers

Ivan Dolog, Robert R. Mallik,[a] Dan Malz, and Anthony Mozynski

*Department of Physics, The University of Akron, Akron, Ohio 44325-4001*

Ultrathin oxygenated amorphous CdTe (*a*-CdTe:O) films are prepared by rf sputtering of CdTe in a background of argon or argon/nitrogen/oxygen mixtures. Atomic force microscopy (AFM) is used to characterize the films and shows that they have an island structure typical of most sputtered thin films. However, when sufficiently low powers and deposition rates are employed during sputtering, the resulting films are remarkably smooth and sufficiently thin for use as barrier layers in inelastic electron tunneling (IET) junctions. Four terminal current–voltage data are recorded for Al/*a*-CdTe:O/Pb tunnel junctions and conductance–voltage curves are derived numerically. WKB fits to the conductance–voltage curves are obtained using a two-component trapezoidal plus square (TRAPSQR) model barrier potential to determine values for the tunnel barrier parameters (height, shape, and width); these parameters are consistent with AFM topological measurements and values from similar devices reported in the literature. IET spectra are presented which confirm that electrons tunnel through ultrathin regions of the *a*-CdTe:O films, which contain aluminum oxide subregions in a manner consistent with the TRAPSQR barrier model. Because tunneling occurs predominantly through these ultrathin regions, IET spectroscopic data obtained are representative of states at, or within a few tenths of nanometers from, the surface and confirm that the *a*-CdTe:O surface stoichiometry is very sensitive to changes in the argon/oxygen/nitrogen concentration ratios during film growth. Full IET spectra, current–voltage, and conductance–voltage data are presented together with tunnel barrier parameters derived from (WKB) fits to the data. The results presented here indicate that inelastic electron tunneling spectroscopy is a useful tool for characterizing the surface states of *a*-CdTe:O and possibly other photovoltaic materials. © *2004 American Institute of Physics.* [DOI: 10.1063/1.1647259]

## I. INTRODUCTION

CdTe is one of the most promising semiconductor materials for high-efficiency thin-film photovoltaic cells. It has a direct band gap in the range 1.4–1.5 eV, which is near the maximum solar energy conversion point. Other advantages of this material are its relatively high efficiency and low price. For the manufacture of photovoltaic devices, CdTe films need to be only 2–10 $\mu$m thick, since most optical absorption takes place within the first 2 $\mu$m of the CdTe surface. However, as with all thin film devices, decreasing the film thickness increases the surface area to volume ratio, which in turn increases the significance of surface defect states. In this article, we investigate the surface states of CdTe by performing measurements on extremely thin regions of sputtered amorphous CdTe films.

CdTe films can be deposited in a number of ways, such as sintering of screen-printed layers,[1] electrodeposition,[2] evaporation,[3] closed space sublimation,[4] and chemical vapor deposition.[5] Sputtering is an alternative method for fabricating CdTe solar cells. It is easy realized and one of the most scalable deposition techniques for large area coatings. At present, the best efficiency reported (16%) was by Aramoto *et al.*,[6] for a CdS/CdTe heterostructure grown by a mixed technique. The maximum efficiency for a thin film CdTe solar cell in which both semiconductor layers were deposited by planar magnetron rf sputtering is 11.6%. However, it is believed that more than 13% efficiency can be achieved using this method.[7]

Considerable compositional and stoichiometric changes may occur when films are prepared in the presence of oxygen. Small amounts of oxygen allow films to maintain their initial properties and may be helpful for optoelectronic devices, playing the role similar to $SiO_2$.[8] It was reported in 1991 that it is possible to incorporate oxygen in CdTe structures by using rf sputtering in a background of argon, nitrogen and oxygen;[8] a compound, amorphous oxygenated cadmium telluride (*a*-CdTe:O) prepared in this way, can be used in many optoelectronic devices. Also, by varying the argon/nitrogen/oxygen ratio while sputtering, the band gap energy and electrical resistivity can be tailored. Values ranging from 1.48 to 3.35 eV and from $10^4$ to $10^{12}$ $\Omega$ cm, respectively, have been reported in the literature.[8]

Although the maximum theoretical efficiency for *a*-CdTe:O solar cells was found to be over 29%, the best reported numbers for actual materials are far from that.[9] It may be possible to enhance performance if the various processes in the bulk of material and on the interfaces can been identified and understood. Several techniques have been used to investigate these processes including x-ray photoelectron

---
[a]Author to whom correspondence should be addressed; electronic mail: rrm@physics.uakron.edu

spectroscopy,[10] and deep level transient spectroscopy.[11] In this article, we use inelastic electron tunneling spectroscopy (IETS), which been used previously to study the vibrational spectra of ultrathin sputtered films of germanium oxide,[12] silicon and its oxides,[13,14] and evaporated silicon and its oxides.[15] In this technique, inelastic scattering of electrons tunneling through a thin-film barrier in a metal/barrier/metal tunnel junction is employed to excite vibrational, optical, and electronic modes in the barrier material. Using IETS to study thin films has an advantage over Raman and IR spectroscopy because the signal to noise ratio for IETS increases for thinner adsorbed layers, whereas it decreases for Raman and IR. This enhances the ability of IETS to detect surface states. Also, optically forbidden modes can be observed as strong peaks. IETS can detect fractional monolayer coverage and has been used to study many complex systems.[16]

The IET barrier parameters (height and width) have a great influence on the elastic and inelastic components of the tunnel current. This influence can be investigated by modeling the metal/barrier/metal system using the WKB approximation. This has been done for alumina tunnel barriers with and without adsorbed molecular layers.[17–19] However, the literature indicates this has not been done for CdTe IET barriers. In this article, we present results of a study of thin, $a$-CdTe:O films using IETS. We also determine model tunnel barrier parameters such as height, width, and shape using the WKB approximation.

Atomic force microscopy (AFM) has been widely used to characterize surface of thin semiconductor films[14] and other materials. We also employed AFM to characterize the topology of the $a$-CdTe:O film and to assist in extracting values for parameters needed for the barrier modeling in subsequent WKB approximations.

## II. EXPERIMENT

### A. Tunnel junction fabrication

Tunnel junctions were prepared on precleaned glass microscope slides in a stainless steel vacuum chamber at a base pressure of $\sim 10^{-6}$ Torr. Prior to junction fabrication the chamber was cleaned by exposure to an oxygen and/or argon plasma discharge and the sputter target was run for approximately 10 min to remove possible surface contamination. Then aluminum base electrodes, approximately 100 nm thick, were then evaporated onto the microscope slide with their geometry defined by a shadow-mask. Next, the insulating barrier was formed. Depending on the desired sample, this was done by exposure of the aluminum film to one, or a sequential combination of, the following procedures.

(a) rf sputtering of CdTe. A 2 in. diameter 0.25 in. thick 99.999% pure CdTe target, supplied by Kurt J. Lesker Company was used. Sputtering was performed in a background of argon with chamber pressure in the range 50–60 mTorr. rf power was in the range of 5 W, yielding deposition rates of approximately 0.01–0.02 nm/s.

(b) rf sputtering of CdTe with the same target and conditions, but performed in a background of argon/nitrogen/oxygen.

Typical average CdTe film thicknesses were of the order of 10 nm as measured by a quartz-crystal thickness monitor. Finally, the tunnel junctions were completed by the evaporation of lead cover electrodes approximately 300 nm thick. Source materials used for the preparation of the electrodes were 99.999% pure or better.

### B. AFM

The topology and surface roughness of the CdTe films, sputtered onto aluminum films of the type used for our IETS measurements, were determined with a Digital Instruments Nanoscope II operating in constant force mode and using standard SiN tips.[20] AFM images were recorded under ambient conditions with the instrument housed in a class-100 clean room. For comparison, the underlying aluminum films were also imaged.

### C. IETS measurements

First, junction resistances were recorded using a four-terminal technique. Spectra were then recorded for junctions with resistances in a suitable range (a few ohms to a few hundred ohms). Full details of our spectrometer are reported elsewhere[21] so only a brief description is present here. Junctions were cooled to 4.2 K in liquid helium and then, in order to verify that tunneling was the predominant conduction mechanisms through the CdTe barrier, low bias features characteristic of the Pb superconducting band gap were recorded. Spectra were then collected by signal averaging over 20 scans. Normalized tunneling intensity measurements were recorded by operating our spectrometer in constant resolution mode.[22]

### D. *I–V* and conductance–voltage measurements

Four terminal $I-V$ measurements were performed, and the data were recorded using a commercially available data acquisition software package. Conductance–voltage ($G-V$) data were derived numerically from the $I-V$ measurements, where $G=dI/dV$.

## III. RESULTS AND DISCUSSION

### A. AFM

Figure 1(a) shows an AFM image of a typical 16 nm film of $a$-CdTe:O sputter deposited onto a thin film aluminum electrode supported on a microscope slide. Commercially available imaging software[23] was used to characterize the film. A familiar granular structure is observed, similar to most sputtered films, which forms by nucleation and growth. The grain size is approximately 40–70 nm, the root-mean-square surface roughness is calculated to be 1.15 nm, and the maximum peak-to-peak height is 11.2 nm. The ten-point height (i.e., the average height of the five highest local maxima plus the average height of the five lowest local minima) is found to be 8.5 nm. This value represents the average roughness in the vicinity of gaps and voids in the film.

Figure 1(b) shows an AFM image of an aluminum film, of the type used for our IETS measurements, evaporated
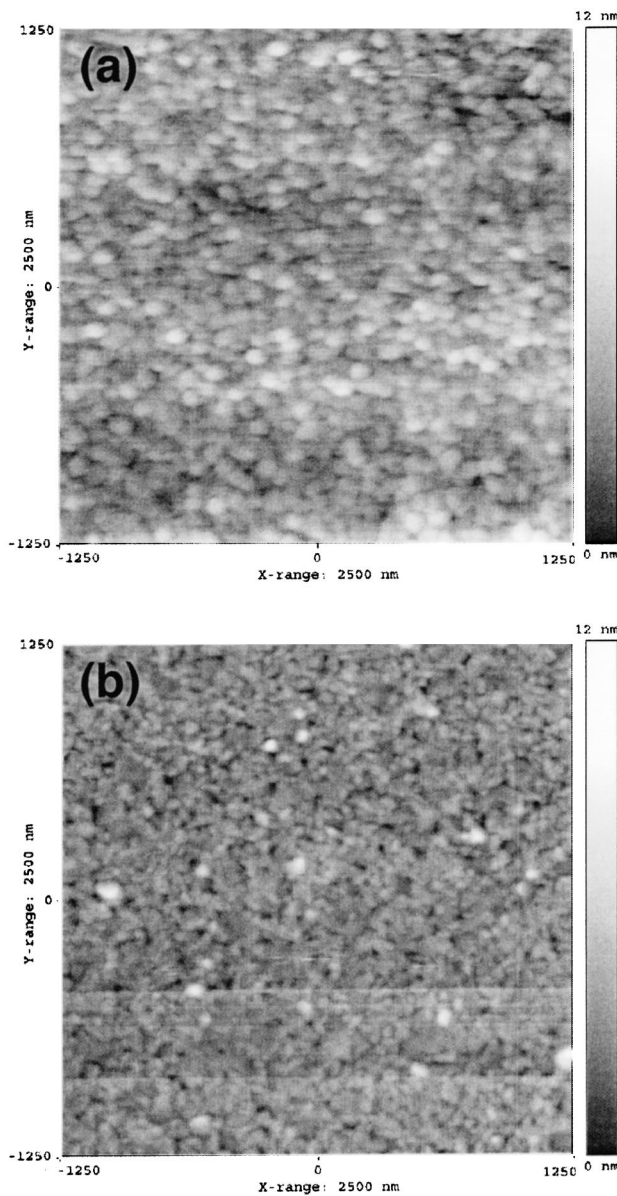
FIG. 1. (a) AFM image of a 16-nm-thick $a$-CdTe:O film sputtered onto a thin-film aluminum electrode supported on a glass microscope slide. The $a$-CdTe:O film shows structure typical of island growth. The islands are approximately 11-nm-thick ($z$ direction) and 40–70 nm diameter ($x–y$ plane). (b) AFM image of a ~100 nm aluminum film, of the type used for the present IETS measurements, evaporated onto a glass microscope slide. This is representative of the structure below that of Fig. 1(a).



FIG. 2. Schematic cross section of an Al/$a$-CdTe:O/Pb tunnel junction (not to scale) indicating nominal film thicknesses. Thicknesses for the aluminum and lead electrode films are not critical. The average thickness of the $a$-CdTe:O island layer is determined by a quartz crystal monitor. IET spectral data and WKB fits to tunneling conductance–voltage measurements indicate that nanoscale subregions of alumina are interspersed as shown.

lieve an idealized cross-section of the IET junctions can be represented schematically as shown in Fig. 2. We believe thin regions of aluminum oxide exist on the aluminum electrode, while clusters of $a$-CdTe:O form to create a quasicontinuous granular film. For subsequent modeling of the tunnel barrier (see Sec. III B later) we assume that tunneling occurs predominantly through regions containing both alumina and $a$-CdTe:O as indicated by the arrows in Fig. 2.

## B. Model barrier parameter calculations

A typical $I$–$V$ curve for an Al/$a$-CdTe:O/Pb tunnel junction is shown in Fig. 3. The junctions are remarkably linear up to about $\pm0.6$ V with an approximately 10%–30% change in the conductance (the magnitude of the change depends on whether the junction is under forward or reverse

onto a clean glass microscope slide. As can be seen, a much finer granular structure is observed. From this we can be sure that the larger islands observed in Fig. 1(a) are indeed $a$-CdTe:O.

In order to record tunnel currents sufficiently large for IETS, it is necessary for the effective barrier thickness to be of the order of $<3$ nm. Since we are able to record IET spectra (see Sec. III C later) it is evident that tunneling does not take place uniformly through the entire barrier, which has an average thickness of approximately 10 nm. Rather, tunneling occurs preferentially through thinner regions of the tunnel barrier. Based upon the AFM characterization of our films (earlier), and subsequent IET measurements, we be-
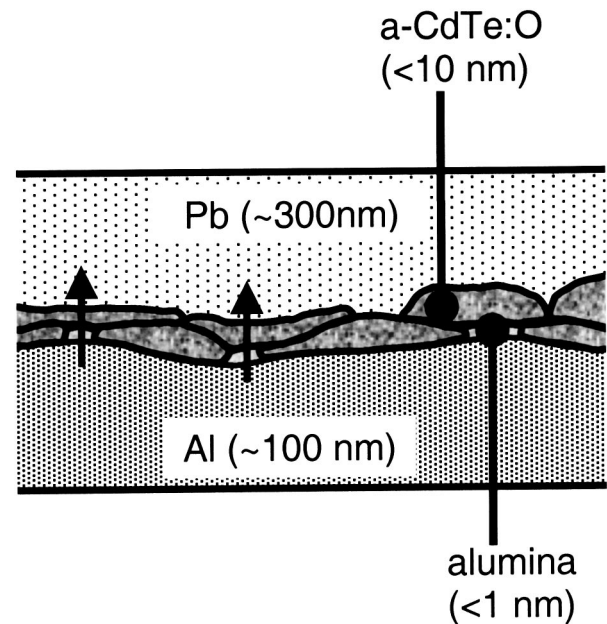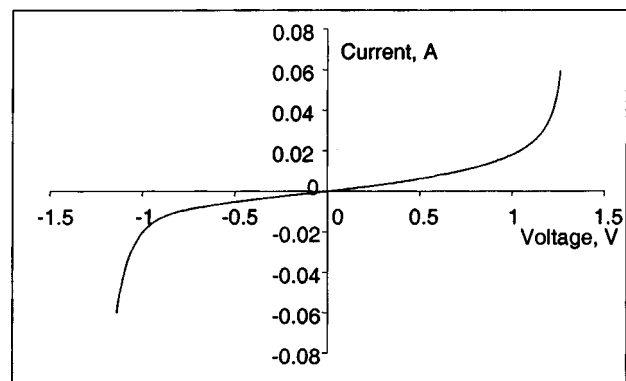


FIG. 3. Typical $I$–$V$ curve for an Al/$a$-CdTe:O/Pb tunnel junction. The slope change from 0 V to approximately $\pm0.6$ V is typically 10%–30% and is asymmetric with bias polarity.
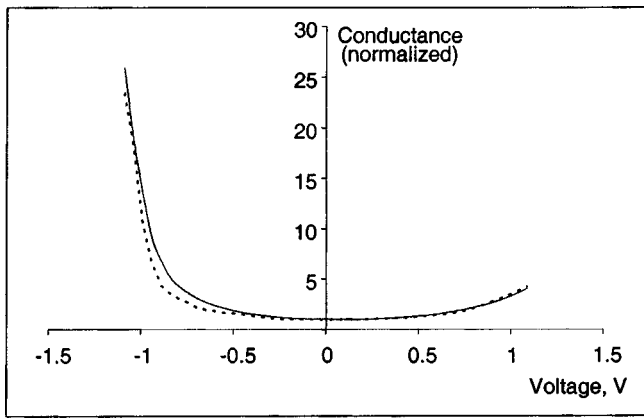
FIG. 4. Normalized conductance–voltage dependence recorded for an Al/$a$-CdTe:O/Pb tunnel junction (dashed line), and fit to the data using a WKB approximation (solid line). See Fig. 5 for details of the WKB approximation.

bias). However, at higher voltages exponential behavior is observed. The derivative of the curve was obtained numerically to give the $G–V$ plot of Fig. 4 (dashed line). Further evidence to support the structure shown in Fig. 2 can be provided by model barrier parameter calculations. We have performed WKB approximations, utilizing a computer fitting procedure. First, to minimize effects due to experimental noise, a standard least-squares function from a commercially available software package (MATLAB) was used to obtain a fit to the experimental normalized $G–V$ curves.

The WKB fit (solid line in Fig. 4) to this smoothed curve was then obtained as follows. The WKB approximation to the tunnel current density is given by

$$j = \frac{2e}{h} \int_{-\infty}^{\infty} \exp\left( -\frac{2}{\hbar} \int_0^{d+s} \{2m[\varphi(x,V)-E_x]^{1/2}\}dx \right)$$
$$\times [f(E)-f(E-eV)]dE_x,$$

where the $h$ is Planck's constant, $\hbar = h/2\pi$, $e$ is the electronic charge, $x$ is the distance into the barrier, $d+s$ is the total thickness of the barrier, $E$ is the total energy of the tunneling electrons, $E_x$ is the $x$ component of the energy, and $\varphi(x,V)$ describes the barrier potential. A trapezoidal plus square TRAPSQR barrier was used (see Fig. 5) since this model is
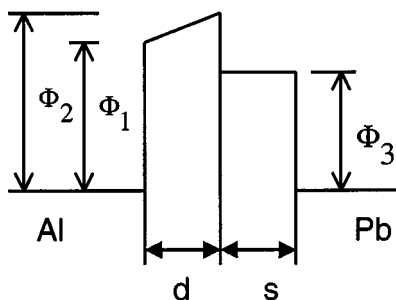
known to give a reasonable fit for systems similar to ours.[15–17] Using a linear distribution of voltage $\varphi(x,V)$ has the form

$$\varphi(x,V) = \Phi_1 + (\Phi_2 - \Phi_1)x/d - (x/d+s)V,$$
$$\text{when} \quad 0 \leq x \leq d, \quad \text{and}$$

$$\varphi(x,V) = \Phi_3 - \left(\frac{x}{d+s}\right)V, \quad \text{when} \quad d \leq x \leq d+s.$$

The normalized conductance was obtained by numerical differentiation of the tunneling current and varying the five adjustable barrier parameters to produce the best fit to the experimental data. Clearly there are many possible values of these parameters that will produce a fit but some of these represent situations that are physically unrealistic. For example, one solution requires that $d$ and $s$ are both less than 0.1 nm, therefore, based upon known values for aluminum oxide barriers with and without adsorbed molecular layers[16,17] and our proposed tunnel junction structure based on IETS and AFM measurements, we believe the following parameters (which produce the solid line fit to the data in Fig. 4) are highly reasonable: $\Phi_1 = 1.7$ V, $\Phi_2 = 2.61$ V, $\Phi_3 = 0.88$ V, $d = 0.25$ nm, and $s = 0.49$ nm. These values of $\Phi_1$, $\Phi_2$, $\Phi_3$, $d$, and $s$ were obtained from the solution that represents the most realistic and plausible physical values for these parameters. The fit is good when one considers that it is possible that some tunneling may occur through regions consisting of $a$-CdTe:O only, which we have ignored in our model. The values obtained for the barrier parameters are consistent with the physical constraints at the surface of CdTe known to produce changes in the barrier heights as compared to the bulk values in a manner similar to other amorphous thin films[17] and also previous work on alumina tunnel barrier heights.[19] It has been shown that effects such as the presence of grain boundaries and associated surface strains can lower barrier heights[24] leading to values of approximately 0.8 eV for doped polycrystalline CdTe films. Sarmah and Rahman[25] found that for Schottky barriers formed by sputtering Cd doped with Cd metal onto Ag, Al, or Ni, the barrier heights are approximately 0.6–0.7 eV. One would expect undoped and partly oxidized CdTe films, as is the case in the present work, to exhibit slightly higher barrier heights than doped polycrystalline materials as we observe. Thus our value for the CdTe barrier height ($\Phi_3$) of 0.88 V obtained from WKB fits to inelastic electron tunneling $G–V$ measurements is in good agreement with the literature.

As mentioned in Sec. III A, we believe that tunneling occur predominantly through the thinner regions of the tunnel barrier as indicated by the arrows in Fig. 2. These regions are formed during the sputtering process and are comprised of small subregions of alumina "capped" by $a$-CdTe:O. At first sight, the barrier thicknesses obtain from the WKB fits may appear to be rather low. However, and for comparison purposes, the barrier thicknesses and heights we obtain by modeling the barrier in this way are not wildly unlike those obtained by other workers using a similar method for organic doped alumina barriers. For example, Walmsley *et al.*[26] have investigated Al/alumina/$m$-cresol/Pb IET junctions. They define the parameters $\Phi_1$, $\Phi_2$, $\Phi_3$, $d$, and $s$ for their insulating



FIG. 5. Schematic energy diagram for an Al/$a$-CdTe:O/Pb tunnel junction assuming a TRAPSQR barrier under zero bias, where $d$ and $s$ refer to the thicknesses of the alumina and $a$-CdTe:O layers, respectively. Barrier heights for the layers are indicated.
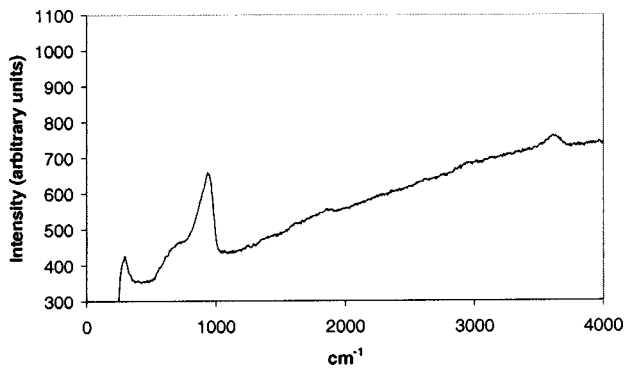
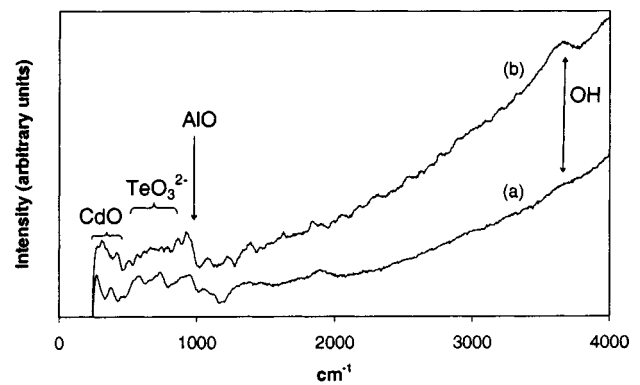FIG. 6. Control IET spectrum obtained from an Al/alumina Pb junction.



FIG. 7. IET spectra obtained from Al/$a$-CdTe:O/Pb junction prepared in (a) argon and (b) a mixture of argon/nitrogen/oxygen. The average thickness of the $a$-CdTe:O layer is approximately 7 nm.

TRAPSQR barrier in the same sense as ours and obtain the best fit to their experimental conductance curves with values of $\Phi_1 = 0.70$ V, $\Phi_2 = 4.2$ V, $\Phi_3 = 8.8$ V, $d = 0.845$ nm, and $s = 0.253$ nm. This means their alumina/$m$-cresol layer is modeled by an approximately 1.1-nm-thick barrier. This barrier is certainly thicker than ours since the Al films were exposed to air then doped with an organic compound ($m$-cresol). Also, Dragoset *et al.*[27] have modeled the barrier layer of Al/alumina/cytidine-5′-monophosphate/Pb IET junctions using much the same method. Their junctions had higher resistances than ours (770–4600 $\Omega$) and parameters were obtained of the order $\Phi_1 \sim 3.5$–5.3 V, $\Phi_2 \sim 4.6$–5.6 V, $\Phi_3 \sim 5.0$–7.3 V, $d \sim 0.93$–0.96 nm, and $s \sim 0.15$–0.18 nm (the values depend on the water vapor content of the barriers). So these workers' model barriers are approximately 1.1 nm thick. Therefore, the thickness values we obtain ($\sim 0.7$ nm), from WKB fits to our primarily semiconducting barriers, comprised of thin alumina subregions capped by $a$-CdTe:O, are not excessively low while the mean barrier height is lower than for insulating barriers as one would expect.

## C. IET spectra

Figure 6 is a control spectrum obtained from an Al/alumina/Pb junction and reveals that there is no contamination present in the alumina layer. The only peaks present are at $\sim 300$ cm$^{-1}$ (an Al metal phonon associated with the Al electrode), 950 cm$^{-1}$ due to Al–O phonon vibrations, a broad peak at 3628 cm$^{-1}$ due to stretching of Al–OH surface hydroxyl groups, and weak bending modes of the Al–OH groups around 720 cm$^{-1}$

Figure 7 shows two spectra obtained from Al/$a$-CdTe:O/Pb tunnel junctions. In both cases the average thickness of the $a$-CdTe:O layer was approximately 7 nm. The first spectrum, Fig. 7(a), was obtained from a film deposited by sputtering in a background of argon while the other, Fig. 7(b), was deposited in a mixture of equal parts argon/nitrogen/oxygen, which is believed to produce an $a$-CdTe:O film.[8,28] Figure 7(b) is representative of many tens of spectra we have recorded for $a$-CdTe:O films deposited in argon/nitrogen/oxygen background mixtures, and is much noisier than that of Fig. 7(a). It is known that when nitrogen is introduced during the sputtering of CdTe, it catalyzes the incorporation of oxygen into the films.[29] This oxidation step

may produce more defects in the films which may be responsible for the extra noise in the spectra. Unfortunately this makes comparisons between the spectra more difficult.

As mentioned in the introduction, it is known that small variations in the ratios of argon/nitrogen/oxygen can produce noticeable differences in the film composition.[8] Also evident is that very small amounts of nitrogen and oxygen are required. This is evident when one compares Figs. 7(a) and 7(b). The spectra are similar, indicating that even without the addition of oxygen and nitrogen there were enough residual amounts of these gases in the chamber to oxidize the $a$-CdTe during the sputtering process (which is performed with a chamber pressure of a few tens of milliTorr). Therefore, we can conclude that all our samples have an $a$-CdTe:O film as the barrier material between the two metal electrodes. Figure 8 shows an expanded region (0–1500 cm$^{-1}$) of Fig. 7. It is hard to define all peaks due to the complexity of the system; nevertheless, the shoulder at 276 cm$^{-1}$ and peak at 384 cm$^{-1}$ are due to TO and LO CdO phonons, respectively.[30,31] Others peaks are due to phonons associated with the $a$-CdTe:O matrix such as TeO$_3^{2-}$ phonons which appear in the spectra as small features at 600 cm$^{-1}$ [$v_3(E)$], and 700 cm$^{-1}$ [$v_3^1(E)_s$], and the shoulder at 750 cm$^{-1}$ [$v_1(A_1)$].[32] In both spectra Al–O and $a$-CdTe:O peaks are present, however, the relative intensities are different. Peaks related to Al–O such as the phonon mode at 950 cm$^{-1}$ and stretching of Al–OH bonds at
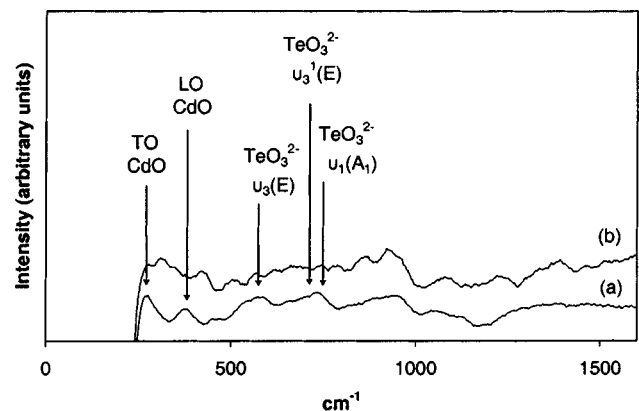


FIG. 8. Expanded region of Fig. 7 showing peak assignments.

$3628$ cm$^{-1}$ are more noticeable in the second spectra, Fig. 7(b), since more oxygen is present in the chamber during preparation.

## IV. CONCLUSIONS

Remarkably smooth ultrathin films, suitable for IET spectroscopy, can be produced by sputtering commercially available CdTe source material in a background of either argon or argon/nitrogen/oxygen. AFM measurements presented here have shown that the films exhibit an island structure, with typical island dimensions of 40–70 nm in the $(x-y)$ plane of the IET junction, and $\sim 10$ nm in the $z$ direction. Electron tunneling $G-V$ measurements provide evidence that electrons tunnel predominantly through thinner regions of the films, as one would expect. IET spectroscopic measurements indicate that these regions, which are representative of the surface of the sputtered films, are composed of $a$-CdTe:O and incorporate interspersed nanoscale subregions of aluminum oxide. IETS confirms that the stoichiometry of these regions is very sensitive to small fluctuations in the argon/nitrogen/oxygen concentrations during film growth. Notwithstanding the complexities of determining the exact composition of the barrier material, it is possible to obtain reasonable WKB fits to the experimental $G-V$ curves by assuming a simple two-component TRAPSQR barrier model comprising of the $a$-CdTe:O islands and alumina subregions. WKB fits are achieved by using values for the effective tunnel barrier region thicknesses, based on AFM topological measurements, and heights based on plausible values from the literature suitably modified to take into account surface effects and compositional changes. To summarize, we have shown that the combination of AFM, IETS, and tunneling $G-V$ measurements provide self-consistent results which are very useful for determining the composition and topology of ultrathin sputtered $a$-CdTe:O films, and, by extension, possibly other photovoltaic materials.

## ACKNOWLEDGMENTS

[1] H. Uda, A. Nakano, K. Kuribayashi, Y. Komatsu, H. Matsumoto, and S. Ikegami, Jpn. J. Appl. Phys., Part 1 **22**, 1822 (1983).

[2] B. M. Basol and E. S. Tseng, Appl. Phys. Lett. **48**, 946 (1986).

[3] R. W. Birkmire, L. C. DiNetta, D. C. Jackson, P. G. Laswell, B. E. McCandless, J. D. Meakin, and J. E. Philips, Proc. 18th IEEE Photovolt. Spec. Conf., Las Vegas, 1985, p. 1413.

[4] K. W. Mitchell, C. Eberspacher, F. Cohen, J. Avery, G. Duran, and W. Bottenberg, Proc. 18th IEEE Photovolt. Spec. Conf., Las Vegas, 1985, p. 1359.

[5] T. L. Chu, S. S. Chu, F. Firszt, H. A. Naseem, R. Stawski, and G. Xu, Proc. 18th IEEE Photovolt. Spec. Conf., Las Vegas, 1985, p. 1643.

[6] T. Aramoto *et al.*, Jpn. J. Appl. Phys., Part 1 **36**, 6304 (1997).

[7] M. Shao, A. Fischer, D. Grecu, U. Jayamaha, E. Bykov, G. Contreras-Peunte, R. G. Bohn, and A. D. Compaan, Appl. Phys. Lett. **69**, 3045 (1996).

[8] F. J. Espinoza *et al.*, Jpn. J. Appl. Phys., Part 2 **30**, L1715 (1991).

[9] A. De Vos, J. E. Parrot, P. Baruch, and P. T. Landsberg, 14th European Photovoltaic Solar Energy Conf., Amsterdam, 1994, p. 1315.

[10] M. Y. El Azhari, M. Azian, A. Bennouna, A. Outzourhit, E. L. Ameziane, and M. Brunel, Thin Solid Films **295**, 131 (1997).

[11] F. A. Abulfotuh, A. Balcioglu, T. Wangensteen, H. R. Moutinho, F. Hassoon, A. Al-Douri, A. Alnajjar, and L. L. Kazmerski, 26th IEEE Photovoltaic Specialists Conference, Anaheim, CA, 1997.

[12] R. R. Mallik, S. Anabtawi, B. Moore, and T. A. Hartman, Surf. Sci. **380**, 124 (1997).

[13] R. R. Mallik, T. Butler, Jr., W. J. Kulnis, Jr., and B. DeVier, J. Appl. Phys. **73**, 2347 (1993).

[14] R. R. Mallik, P. N. Henriksen, T. Butler, Jr., W. J. Kulnis, Jr., and T. Confer, J. Vac. Sci. Technol. A **10**, 2412 (1992).

[15] M. Higo, K. Nishino, and S. Kamata, J. Phys. Chem. **96**, 1848 (1992).

[16] U. Mazur and K. W. Hipps, in *Handbook of Vibrational Spectroscopy*, edited by John Chalmers and Peter Griffiths (Wiley, New York, 2001), Vol. 1, pp. 812–829 (invited review article).

[17] L. D. Bell and R. V. Coleman, Phys. Rev. B **30**, 4120 (1984).

[18] R. V. Coleman, L. D. Bell, R. A. Dragoset, A. M. Johnson, H.-A. Lu, and E. S. Phillips, Phys. Rev. B **29**, 4246 (1984).

[19] R. B. Floyd and D. G. Walmsley, J. Phys. C **11**, 4601 (1978).

[20] MikroMasch, Narva mnt. 13, 10151 Tallinn, Estonia.

[21] R. R. Mallik, Y. Wang, and P. N. Henriksen, Rev. Sci. Instrum. **64**, 890 (1993).

[22] T. R. Seman and R. R. Mallik, Rev. Sci. Instrum. **70**, 2808 (1999).

[23] Scanning Probe Image Processor (Image Metrology ApS).

[24] L. M. Woods, D. H. Levi, V. Kaydanov, G. Y. Robinson, and T. K. Ahrenkiel, NREL/CP-520-23915, July 1998.

[25] P. C. Sarmah and A. Rahman, Bull. Mater. Sci. **24**, 411 (2001).

[26] D. G. Walmsley, R. B. Floyd, and W. E. Timms, Solid State Commun. **22**, 497 (1977).

[27] R. A. Dragoset, E. S. Phillips, and R. V. Coleman, Phys. Rev. B **26**, 5333 (1982).

[28] F. J. Espinoza-Beltran, R. Ramirez-Bon, J. Gonzalez-Hernandez, F. Sanchez-Sinencio, O. Zelya-Angel, J. G. Mendoza-Alvarez, and G. Torres-Delgado, J. Phys.: Condens. Matter **5**, A345 (1993).

[29] F. J. Espinoza-Beltran, O. Zelaya, F. Sanchez-Sinencio, J. G. Mendoza-Alvarez, M. H. Farias, and L. Banos, J. Vac. Sci. Technol. A **11**, 3062 (1993).

[30] K. H. Rieder, M. Ishigame, and L. Genzel, Phys. Rev. B **6**, 3804 (1972).

[31] I. Giaver and H. R. Zeller, Phys. Rev. Lett. **21**, 1385 (1968).

[32] B. K. Rai, H. D. Bist, R. S. Katiyar, K.-T. Chen, and A. Burger, J. Appl. Phys. **80**, 477 (1996).